Hindawi
Shock and Vibration
Volume 2017, Article ID 2716251, 16 pages
https://doi.org/10.1155/2017/2716251

Research Article

Dynamic Shift Coordinated Control Based on Motor Active Speed Synchronization with the New Hybrid System

Ting Yan,[1] Lin Yang,[1] Bin Yan,[1] Wei Zhou,[1] Liang Chen,[2] and Wei Zhou[1]

[1]*Institute of Automotive Electronic Technology, School of Mechanical Engineering, Shanghai Jiao Tong University, Shanghai 200240, China*
[2]*Shanghai 01 Power Technology Co., Ltd., Shanghai 200240, China*

Correspondence should be addressed to Lin Yang; yanglin@sjtu.edu.cn

Received 1 November 2016; Accepted 10 April 2017; Published 11 July 2017

Academic Editor: Mario Terzo

Considering the inherent disadvantages that severely affect driving comfortability during the shift process in HEVs, a dynamic shift coordinated control based on motor active speed synchronization is proposed to improve shift quality by reduction of shift vibration. The whole control scheme is comprised of three phases, preparatory phase, speed regulation phase, and synchronization phase, which are implemented consecutively in order. The key to inhibiting impact and jerk depends on the speed regulation phase, where motor active speed synchronization is utilized to reach the minimum speed difference between the two ends of synchronizer. A new hybrid system with superior performances is applied to present the validity of the adopted control algorithm during upshift or downshift, which can represent planetary gear system and conventional AMT shift procedure, respectively. Bench test, simulation, and road test results show that, compared with other methods, the proposed dynamic coordinated control can achieve shifting control in real time to effectively improve gear-shift comfort and shorten power interruption transients, with robustness in both conventional AMT and planetary gear train.

1. Introduction

Hybrid electric vehicle (HEV) is emerging as an important substitution for traditional transportation due to its fuel economy improvement and emission reduction. Its powertrain can be classified as conventional AMT type and planetary gear train type based on coupled manner. A new type of hybrid system is proposed in this paper, whose structure combines both of the two mainstream types together, with superiority in dynamic performance and fuel economy as well [1–3]. However, since they have complicated powertrain structure and various operational modes, power interruption and torque fluctuation during mode transformation, especially in the shift synchronization period, can easily result in driving vibrations and jerks, which greatly influences driving comfortability. Alleviating and damping driving vibrations during gear-shift become one of the key issues in vehicle dynamic switching control [4].

Many approaches have been proposed to find better solutions to overcome the shortcomings in gear-shifting process of HEV. Glielmo et al. raised a hierarchical method based on cascaded and decoupled speed and torque control loops [5]. Shin et al. developed a combined gear-shifting method assisted by motor speed feedback control [6]. Baraszu and Cikanek demonstrated that during the gear-shifting process a motor should provide torque directly to reduce the power interruption time [7]. A combination of Dynamic Programming (DP) and Pontryagin's Minimum Principle (PMP) was utilized in a model predictive controller framework to realize a predictive controller in a receding horizon mode for a PHEV equipped with an AMT [8]. The computational burden and assumption that velocity profile is available ahead limit its application in real-time control. Control strategies used in clutchless gear-change drivelines in hybrid electric vehicles are discussed in [9–11]. This limits the usage of the proposed methods in these literatures to the gear-shifting process related to clutch engagement and the drivability performances cannot be guaranteed. The strategy in electric vehicles equipped with hydraulic combined clutch transmissions in [12] is presented to improve the shift quality.

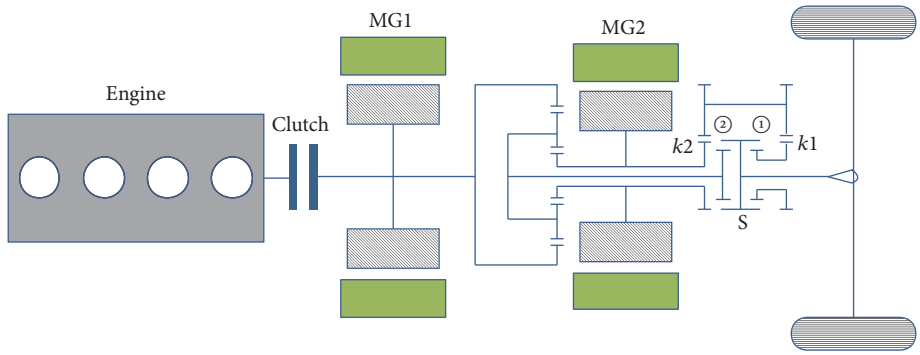

Figure 1: Simplified structural diagram of new HEV system (S: shift synchronizer, MG1: generator, MG2: motor, and $K1/K2$: gear ratio).

Nevertheless, the complexity of the shift hydraulic circuit and its nonlinear feature bring in challenges to predict the oil pressure acting on the brake piston. A synthesis algorithm to realize accurate engine speed control and shift motor position control without disengaging the clutch using engine active control was presented by Zhong et al. [13], which has not significantly improved the conditions on account of the slow response of engine. So motor active speed control was proposed to achieve shifting synchronization during gear-shifting process on account of the rapid response of motor characteristics [14, 15]. However, their powertrain structures are simple, which are both single motor in single axle without clutch, and the algorithms raised cannot be applied to complex powertrains with clutch or dual motors, not to mention with planetary gear system. As a consequence, a new motor active speed synchronization with clutch coordinated control is introduced to achieve a fast and smooth gear-shift in the new hybrid system.

Due to the tremendous structural difference between the two gears of the new hybrid system, the speed difference between the two ends of synchronizer is large as it is ready to shift. Upshift or downshift directly will lead to strong vibrations and severe wear of the synchronizer. As a result, motor speed adjustment is required before the synchronization begins in order to minimize shift time and power interruption period and decrease the impact force and improve shift quality. Meanwhile, to acquire a fast and smooth gear-shift, the engine, motor, clutch, and actuator of the gearbox are controlled precisely and coordinately. Before switching to neural gear, the transmitted torque to the output shaft must be reduced to close to zero; otherwise attempting to disengage or engage the gears which are transmitting large torques can bring about torsional vibration, teeth surface damage of the gears, and synchronization difficulty. So unloading the power sources as well as disengaging the clutch completely is necessary prior to switching to neutral gear. Clutch remains disengaged throughout and motors are unloaded again before the synchronization begins due to the same reason. The coordinated control raised above can ensure the rapidity and smoothness of the gear-shift process as validated by on-board tests.

The dynamic shift coordinated control scheme based on motor active speed regulation can be divided into three phases: unload and switch to neural gear, speed regulation, and mechanical speed synchronization by the synchronizer. The second phase is the core part. The new type of HEV system is employed to assess the feasibility of the control scheme. The reason to select this new hybrid system as the research object depends on two points. Firstly, the new hybrid system has huge advantages in fuel economy and dynamic performances. The rate of fuel saving can reach 17%~28% in different driving cycles in comparison with conventional parallel hybrid vehicles, which can attain up to nearly 40% when compared with traditional diesels [1, 3]. On the other hand, the maximum output torque before the final drive of the new system is over 3600 Nm, which can meet power demands in assorted situations. Secondly, it contains two representative powertrains in two gears and the structural difference between the two gears results in inevitable speed regulation during shift process. By presenting upshift and downshift control scheme, the regulation process in conventional AMT and planetary gear train can both be revealed in the new hybrid system, as shown in Section 3.2. In Section 2, the structure and operating principle of the new HEV system is presented. In Section 3, dynamic coordinated control and active speed synchronization are elaborated, respectively. Bench test and on-board test results showing the effectiveness of the proposed approach are presented in Section 4. Conclusions that summarize the results of the paper are obtained in Section 5.

2. The New HEV System

The simplified structural diagram of the HEV system adopted in this paper is shown in Figure 1. It is mainly composed of a diesel engine, two permanent magnetic motors, and a planetary gear coupling system. MG2 is linked to the sun gear directly, while MG1 is connected to the ring gear and separated from engine by an electronic control clutch. Compared with the traditional hybrid system, the new system can adjust the speed range of engine operating point flexibly through the CVT coupling system, which ensures that engine is working in high-efficiency area and improves vehicle fuel economy. Meanwhile engine can collaborate with generator to drive the vehicle or charge the battery to meet vehicle dynamic and duration requirements.

While the shift synchronizer is placed at the right end, gear number is 1. And the motor output torque is amplified a few times via a conventional gear train to the output shaft to meet the working condition requirement as the demanded torque is high, such as vehicle launching process. As mentioned previously, this relationship can be written as follows:

$$T_f = T_{\mathrm{MG2}} \times K1 \times K2, \tag{1}$$

$$\omega_{f1} = \frac{\omega_{\mathrm{MG2}}}{(K1 \times K2)}, \tag{2}$$

where T_f and T_{MG2} denote the output shaft torque and MG2 torque, respectively, ω_{f1} and ω_{MG2} denote the output shaft speed at the first gear and MG2 speed, and $K1$ and $K2$ denote the gear ratios of the gear train.

While the shift synchronizer is placed at the left end, gear number is 2. The sun gear (MG2) and the ring gear (MG1 and engine) are coupled and transfer torque to the planetary gear ultimately. With the known features of the planetary gear train, the relationship in the steady state is described as follows:

$$T_r = T_{\mathrm{MG2}} \times \alpha, \tag{3}$$

$$T_f = T_r + T_{\mathrm{MG2}} = T_{\mathrm{MG2}} \times (1 + \alpha), \tag{4}$$

$$T_r = T_{\mathrm{MG1}} + \theta \times T_{\mathrm{ICE}}, \tag{5}$$

$$\omega_{f2} = \frac{\alpha \times \omega_{\mathrm{MG1}} + \omega_{\mathrm{MG2}}}{1 + \alpha}, \tag{6}$$

where

$$\theta = \begin{cases} 1, & \text{clutch is engaged} \\ 0, & \text{clutch is disengaged} \\ 0\sim1, & \text{clutch is slipping.} \end{cases} \tag{7}$$

α denotes the coefficient of planetary gear, T_r, T_{MG1}, and T_{ICE} denote the ring gear torque, MG1 torque, and engine torque, respectively, and ω_{MG1}, ω_{ICE}, and ω_{f2} denote MG1 speed, engine speed, and output shaft speed at the second gear.

When the clutch is engaged,

$$\omega_{\mathrm{MG1}} = \omega_{\mathrm{ICE}}. \tag{8}$$

Engine is linked to the powertrain completely in the meantime. From (6) and (8), we can conclude that by adjusting MG2 speed the engine can work in its high-efficiency speed range, leading to vehicle fuel economy improvement, as shown in Figure 2.

While the shift synchronizer is placed in the middle, the powertrain is interrupted. No power can be transferred to the output shaft due to the interruption. It is at the neutral position at this moment.

The operating state of the new HEV system can be divided into four modes. The selection criteria depend on vehicle speed, power requirement, and battery SOC. The four modes are tabulated in Table 1.

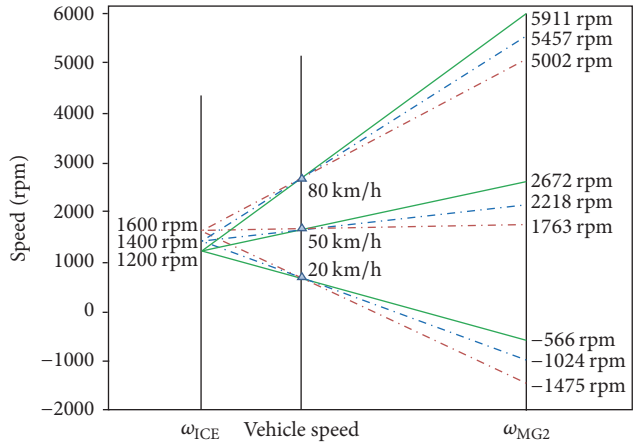

Figure 2: Adjusting MG2 speed to regulate engine operating point.

3. Dynamic Coordinated Control

Coordinated control with other components is indispensable during shift process. It is needed to guarantee the smoothness of synchronization after speed regulation. The whole dynamic coordinated control scheme is composed of three phases, which are shown in Figure 3 and described in detail as follows. Every step in each phase should be confirmed from the feedback of the controlled components before taking on to the next step, which ensures the reliability of the whole procedure.

3.1. Preparatory Phase (Unload and Switch to Neutral Gear). The aim of this phase is to make preparations for the motor active speed regulation. The main task includes unloading power sources, disengaging clutch, and putting into neutral gear. Motors and engine are in no-load condition after being unloaded, which makes it convenient to disengage the clutch later. No torque transmitted to the powertrain helps to switch to neutral gear smoothly to avoid jerks and noise.

The preparatory phase period should not last too long. Otherwise, the driver would perceive the lack of power due to no power output during the phase. On the other hand, the descending slope of the command torque sent to DMCM should be considered not too large, which will induce the feeling of abruption. The flow chart is shown in Figure 4.

3.2. Speed Regulation Phase. Speed regulation during shifting process is indispensable, which is aimed at adjusting the input shaft to a desired speed without overshoot and oscillation. It is found by experiments that only when the speed difference is less than an acceptable reference value ξ can the synchronization start. Moreover, it is easier to put into the target gear when the speed of the active speed-adjusting end is slightly higher than the passive end of the synchronizer, which is in consistence with the principle in conventional buses. So (9) must be satisfied before the synchronization begins:

$$\delta \le \omega_s^T - \omega_s \le \xi, \tag{9}$$

Table 1: The four operation modes of new HEV system.

Mode	Gear number	Clutch status	Description
Single-motor pure electric mode	1	Engaged	Only MG2 drives the vehicle
Series mode	1	Engaged	MG2 drives vehicle; MG1 and engine collaborate to generate electricity
Dual-motor pure electric mode	2	Disengaged	MG1 and MG2 drive the vehicle together
Series-parallel mode	2	Engaged	MG1, MG2, and engine drive the vehicle together

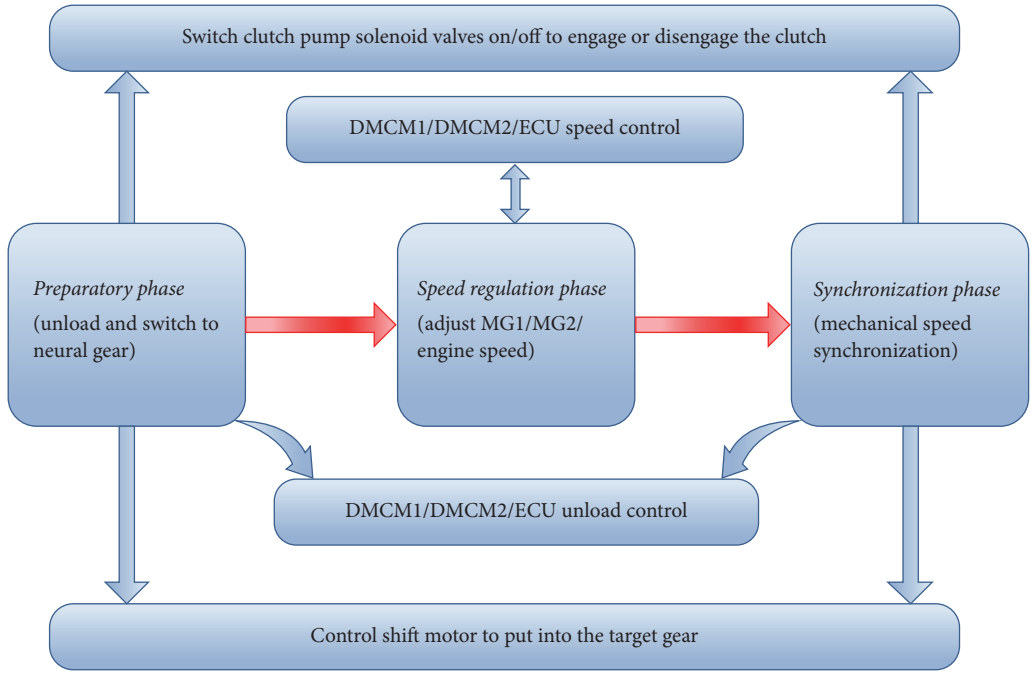

Figure 3: The control scheme of the dynamic coordinated control.

where ω_s^T is the target speed of output shaft linked to the synchronizer in the speed regulation phase, ω_s is actual speed of output shaft, and δ and ξ are speed calibrations determined by the speed difference calibration experiment in the bench test.

The output shaft speed is closely associated with the vehicle speed, as shown in the following equation:

$$\omega_s = \frac{Vss \times i_g}{r} \times \frac{60}{2\pi}, \tag{10}$$

where Vss denotes vehicle speed, i_g denotes final gear ratio, and r denotes the wheel's radius.

Due to short speed-adjusting time, large vehicle rotational inertia, and no power output during the neutral position period, vehicle speed can be assumed to be approximately constant. Then ω_s can be presumed as nearly invariant as well from (10). Equation (11) can be obtained from (2) and (6):

$$\omega_s^T = \begin{cases} \dfrac{\omega_{MG2}^T}{(K1 \times K2)} & \text{downshift} \\ \dfrac{\omega_{MG2}^T + \alpha \times \omega_{MG1}^T}{1 + \alpha} & \text{upshift,} \end{cases} \tag{11}$$

where ω_{MG1}^T and ω_{MG2}^T denote MG1 target speed and MG2 target speed.

The speed regulation processes of upshift and downshift are discussed, respectively, due to the complicated structure of the new HEV system.

3.2.1. The First Upshift Speed Regulation (Single-Motor Mode to Dual-Motor Mode). In single-motor mode, Only MG2

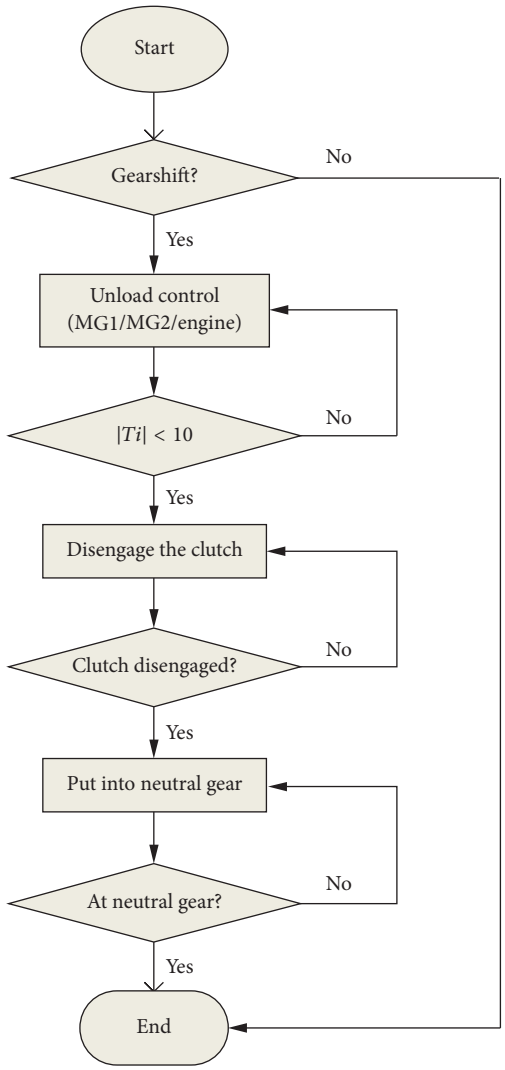

Figure 4: The preparatory phase's flow chart.

propels the vehicle, while engine and MG1 are in idle state and do not output power at all:

$$\omega_{\mathrm{MG1}} = \omega_{\mathrm{ICE}} = 0. \tag{12}$$

In dual-motor mode, MG1 and MG2 propel the vehicle together. One motor must be in speed control mode and the other in torque control mode to keep the system stable due to the features of planetary gear system. MG2 is chosen as the speed controlled motor because of its excellent speed adjustment performance. Then MG1 is in torque control mode as its torque regulation performance is good. The optimal combination of MG2 and MG1 speed of highest system efficiency $(\omega^*_{\mathrm{MG2}}, \omega^*_{\mathrm{MG1}})$ can be acquired based on two motors' efficiency characteristic curves under different vehicle speed and vehicle demanded torque conditions. The calculation procedure is as follows.

(1) Set a combination of vehicle speed and demanded torque (Vss, T_{Dmnd}) as known quantities; then

$$T_{\mathrm{MG1}} = \frac{T_{\mathrm{Dmnd}} \times \alpha}{1+\alpha}, \tag{13}$$

$$T_{\mathrm{MG2}} = \frac{T_{\mathrm{Dmnd}}}{1+\alpha}. \tag{14}$$

(2) Given a series of MG1 speed $(\omega^1_{\mathrm{MG1}}, \omega^2_{\mathrm{MG1}}, \ldots, \omega^n_{\mathrm{MG1}})$, the corresponding MG2 speed under Vss can be conducted $(\omega^1_{\mathrm{MG2}}, \omega^2_{\mathrm{MG2}}, \ldots, \omega^n_{\mathrm{MG2}})$ from the relationship in (6):

$$\omega^k_{\mathrm{MG2}} = \frac{60Vss\,(1+\alpha)\,i_g}{2\pi r} - \alpha\omega^k_{\mathrm{MG1}} \quad k = 1, 2, 3, \ldots, n. \tag{15}$$

(3) MG1 efficiency η^k_{MG1} and MG2 efficiency η^k_{MG2} are gained by making use of the obtained combination $(\omega^k_{\mathrm{MG1}}, T_{\mathrm{MG1}})$ and $(\omega^k_{\mathrm{MG2}}, T_{\mathrm{MG2}})$ to look up to MG1 and MG2 efficiency curves.

(4) If there is a combination $(\omega^i_{\mathrm{MG1}}, T_{\mathrm{MG1}}, \eta^i_{\mathrm{MG1}})$ or $(\omega^i_{\mathrm{MG2}}, T_{\mathrm{MG2}}, \eta^i_{\mathrm{MG2}})$, which meets the equation

$$\frac{\left(\omega^i_{\mathrm{MG1}} \times T_{\mathrm{MG1}}\right)}{\eta^i_{\mathrm{MG1}}} + \frac{\left(\omega^i_{\mathrm{MG2}} \times T_{\mathrm{MG2}}\right)}{\eta^i_{\mathrm{MG2}}} = \min\left[\frac{\left(\omega^k_{\mathrm{MG1}} \times T_{\mathrm{MG1}}\right)}{\eta^k_{\mathrm{MG1}}} + \frac{\left(\omega^k_{\mathrm{MG2}} \times T_{\mathrm{MG2}}\right)}{\eta^k_{\mathrm{MG2}}}\right], \quad (i, k = 1, 2, \ldots, n), \tag{16}$$

then $(\omega^i_{\mathrm{MG1}}, \omega^i_{\mathrm{MG2}})$ is the speed optimal combination $(\omega^*_{\mathrm{MG1}}, \omega^*_{\mathrm{MG2}})$ under (Vss, T_{Dmnd}) conditions.

(5) Repeat the steps above to get all the optimal speed combination $(\omega^*_{\mathrm{MG1}}, \omega^*_{\mathrm{MG2}})$ under different vehicle speed and vehicle demanded torque conditions.

After switching to neutral gear, set MG1 operating in torque controlled mode. Assume that MG1 command torque is T^T_{MG1}; the time from current speed to the target speed $\omega^{\mathrm{raw}}_{\mathrm{MG1}}$ is t_1. MG1 unloads torque and prepares to put into the target gear when reaching the target speed. But MG1 speed will keep on rising up during the unload process because of its response delay until achieving the peak speed. Then it begins to drop slowly. Set the peak speed as ω^p_{MG1} and the period from $\omega^{\mathrm{raw}}_{\mathrm{MG1}}$ to ω^p_{MG1} as t_2. Since MG1 has outstanding torque regulation performance, MG1 actual torque can be considered as achieving the command torque quickly by following a constant slope, as shown in Figure 5.

As MG1 reaches the peak speed, MG1 actual torque is close to zero and the speed change is gentle, which makes it the ideal optimal point.

Set

$$\omega^p_{\mathrm{MG1}} = \omega^*_{\mathrm{MG1}}. \tag{17}$$

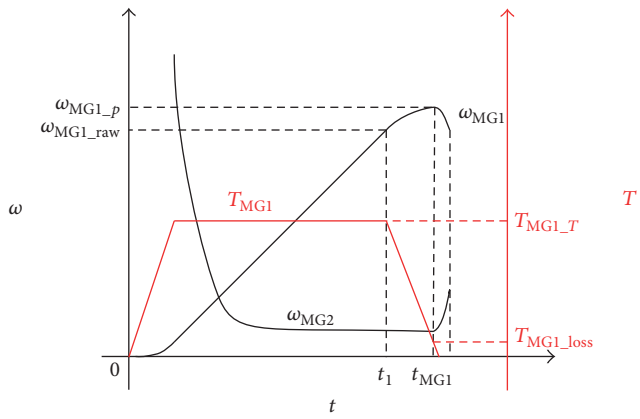

FIGURE 5: Variables changing curves in upshift speed regulation 1.

And the total MG1 speed regulation time is t_{MG1}:

$$t_{MG1} = t_1 + t_2. \tag{18}$$

The speed regulation can be divided into two stages: $0 \sim t_1$ and $t_1 \sim t_{MG1}$. Equation (19) can be obtained in each stage:

$$\begin{aligned} &\frac{(T - T_{loss})^2}{2k} + T\left(t_1 - \frac{T}{k}\right) - T_{loss}t_1 = J\omega_{MG1}^{raw}, \\ &\frac{T^2 - T_{loss}^2}{2k} - T_{loss}\frac{T - T_{loss}}{k} = J\left(\omega_{MG1}^{p} - \omega_{MG1}^{raw}\right), \\ &t_2 = \frac{T - T_{loss}}{k}. \end{aligned} \tag{19}$$

Then t_{MG1} is attained by solving the above equations:

$$t_{MG1} = \frac{(T - T_{loss})}{k} + \frac{\left(T_{loss}^2 - 2TT_{loss} - 2Jk\omega_{MG1}^{p}\right)}{2k(T_{loss} - T)}, \tag{20}$$

where T and T_{loss} denote MG1 command torque and friction torque; k is MG1 torque response slope. J is MG1 equivalent rotational inertia.

The assignment of T should consider that if T is too large, even though t_1 is short, the unloading process is long and speed increment is large. If T is too small, even though unloading time t_2 is short, t_1 will be long due to the small angular acceleration. t_{MG1} will be relatively long in either case. T^* is presumed to be the optimal value of T, which meets the following equation:

$$f\left(T^*, \omega_{MG1}^{p}\right) = \min\left(t_{MG1}\right). \tag{21}$$

Take the partial derivative of T in (20) and T^* is obtained as follows:

$$\begin{aligned} \frac{\partial t_{MG1}}{\partial T} &= \frac{\left(T_{loss}^2 - 2TT_{loss} - 2Jk\omega_{MG1}^{p}\right)}{2k(T_{loss} - T)^2} \\ &\quad - \frac{T}{k(T_{loss} - T)} = 0, \end{aligned} \tag{22}$$

$$T^* = T_{loss} + \sqrt{\frac{T_{loss}^2}{2} + Jk\omega_{MG1}^{p}}. \tag{23}$$

MG2 is set to operate in speed control mode on account of its fast response and regulation precision. By adjusting MG2 target speed ω_{MG2}^{T} quickly, the output shaft speed can be coupled to ω_s^T exactly at the end of speed regulation.

MG2 target speed ω_{MG2}^{T} is

$$\omega_{MG1}^{T} = \begin{cases} \omega_{MG2}^{*} & t \le t_{MG1} \\ (1+\alpha)\,\omega_s^T - \alpha\omega_{MG1} & t > t_{MG1}; \end{cases} \tag{24}$$

namely, MG2 speed is regulated to optimum value ω_{MG2}^{*} prior to MG1 finishing torque regulation, which meets (9) as MG1 rises to the peak speed ω_{MG1}^{*}. If (9) cannot be met during the whole MG1 speed regulation process, then MG2 target speed is modified to satisfy the coupling relationship as MG1 is free falling. The process is close to the shift speed regulation process in planetary gear systems with dual motors.

3.2.2. The Second Upshift Speed Regulation (Single-Motor Mode/Series Mode to Series-Parallel Mode). In series-parallel mode, engine participates in propelling the vehicle. Taking the output shaft speed ω_s, vehicle demanded torque T_{Dmnd}, and engine power P_{ICE} as the known quantity, a three-dimensional function table is made. The object of the function is to acquire the highest combined efficiency of the engine and electrical system and meet the vehicle power requirement and reach SOC control target. The optimal combination $(\omega_{MG2}^{*}, \omega_{MG1}^{*})$ is gained by following the procedure below.

(1) Set the combination $(\omega_s, T_{Dmnd}, P_{ICE})$ as the known quantity. Vehicle demanded power $P_{Dmnd} = T_{Dmnd} \times \omega_s$.

(2) Given a series of MG1 speed $(\omega_{MG1}^{1}, \omega_{MG1}^{2}, \ldots, \omega_{MG1}^{n})$, the corresponding MG2 speed can be obtained as $(\omega_{MG2}^{1}, \omega_{MG2}^{2}, \ldots, \omega_{MG2}^{n})$ under vehicle speed *Vss* condition by the following relationship:

$$\omega_{MG2}^{k} = \omega_s \times (1+\alpha) - \alpha \times \omega_{MG1}^{k} \quad k = 1, 2, 3, \ldots, n. \tag{25}$$

Engine speed is equal to MG1 speed.

(3) Engine torque is given as follows:

$$\begin{aligned} &\left(T_{ICE}^{1}, T_{ICE}^{2}, T_{ICE}^{3}, \ldots, T_{ICE}^{n}\right) \\ &\quad = \left(\frac{P_{ICE}}{\omega_{MG1}^{1}}, \frac{P_{ICE}}{\omega_{MG1}^{2}}, \frac{P_{ICE}}{\omega_{MG1}^{3}}, \ldots, \frac{P_{ICE}}{\omega_{MG1}^{n}}\right). \end{aligned} \tag{26}$$

MG1 command torque is given as follows:

$$\begin{aligned} \left(T_{MG1}^{1}, T_{MG1}^{2}, \ldots, T_{MG1}^{n}\right) &= \left(\frac{T_{Dmnd} \times \alpha}{1+\alpha}\right. \\ &\quad \left. - T_{ICE}^{1}, \frac{T_{Dmnd} \times \alpha}{1+\alpha} - T_{ICE}^{2}, \ldots, \frac{T_{Dmnd} \times \alpha}{1+\alpha} - T_{ICE}^{n}\right). \end{aligned} \tag{27}$$

MG2 torque is given as follows: $T_{MG2} = T_{Dmnd}/(1+\alpha)$.

(4) MG1 efficiency η_{MG1}^{k}, MG2 efficiency η_{MG2}^{k}, and engine efficiency η_{ICE}^{k} are gained by making use of the obtained

combinations $(\omega^k_{MG1}, T_{MG1})$, $(\omega^k_{MG2}, T_{MG2})$, and $(\omega^k_{ICE}, T_{ICE})$ to look up to MG1, MG2, and engine efficiency curves.

(5) If there are combinations $(\omega^i_{MG1}, T_{MG1}, \eta^i_{MG1})$, $(\omega^i_{MG2}, T_{MG2}, \eta^i_{MG1})$, and $(\omega^i_{ICE}, T_{ICE}, \eta^i_{ICE})$ which meet the equation

$$\frac{\left(\omega^i_{MG1} \times T_{MG1}\right)}{\eta^i_{MG1}} + \frac{\left(\omega^i_{MG2} \times T_{MG2}\right)}{\eta^i_{MG2}} + \gamma \times \frac{P_{ICE}}{\eta^i_{ICE}} = \min\left[\frac{\left(\omega^k_{MG1} \times T_{MG1}\right)}{\eta^k_{MG1}} + \frac{\left(\omega^k_{MG2} \times T_{MG2}\right)}{\eta^k_{MG2}} + \gamma \times \frac{P_{ICE}}{\eta^k_{ICE}}\right] \quad (i,k = 1,2,\ldots,n), \tag{28}$$

where γ is the equivalent conversion factor from engine power to electric power, then $(\omega^i_{MG1}, \omega^i_{MG2})$ is the speed optimal combination $(\omega^*_{MG1}, \omega^*_{MG2})$ under (Vss, T_{Dmnd}) conditions.

(6) Repeat the steps above to get all the optimal speed combination $(\omega^*_{MG1}, \omega^*_{MG2})$ under different vehicle speed, vehicle demanded torque, and engine power conditions.

When entering series-parallel mode, clutch has to be engaged as soon as possible. Hence the speed difference between MG1 and engine should not be too big; otherwise engaging directly will result in severe abrasion and jerk. Moreover, readjusting MG1 speed will delay MG1 torque recovery time. To avoid the problems appearing after upshift process, engine speed is always commanded to the optimum speed ω^*_{MG1} during the shift process, which is also the target speed of MG1:

$$\omega^*_{ICE} = \omega^T_{MG1} = \omega^*_{MG1}. \tag{29}$$

MG2 speed regulation target is the same as (24). MG1 command torque in single-motor mode to series-parallel mode is identical to (23). The derivation of T^* in series mode to series-parallel mode is similar to (19) and (22):

$$T^* = \begin{cases} T_{loss} + \sqrt{\dfrac{T^2_{loss}}{2} + Jk\left(\omega^p_{MG1} - \omega^s_{MG1}\right)} & \omega^p_{MG1} > \omega^s_{MG1} \\ T_{loss} - \sqrt{\dfrac{T^2_{loss}}{2} + Jk\left(\omega^s_{MG1} - \omega^p_{MG1}\right)} & \omega^p_{MG1} < \omega^s_{MG1}, \end{cases} \tag{30}$$

where ω^s_{MG1} is MG1 speed in series mode. Unlike the single-motor mode to series-parallel mode, T^* in series mode to series-parallel mode may be positive or negative depending on whether ω^s_{MG1} is less than ω^p_{MG1} or not. The situation when $T^* > 0$ is similar to Figure 4, while $T^* < 0$ is shown in Figure 6.

3.2.3. Downshift Speed Regulation. Only MG2 connects to the powertrain after downshift no matter in single-motor mode or in series mode. MG2 target speed can be obtained in (31), which is similar to conventional AMT:

$$\omega^T_{MG1} = \omega^T_s \times K1 \times K2. \tag{31}$$

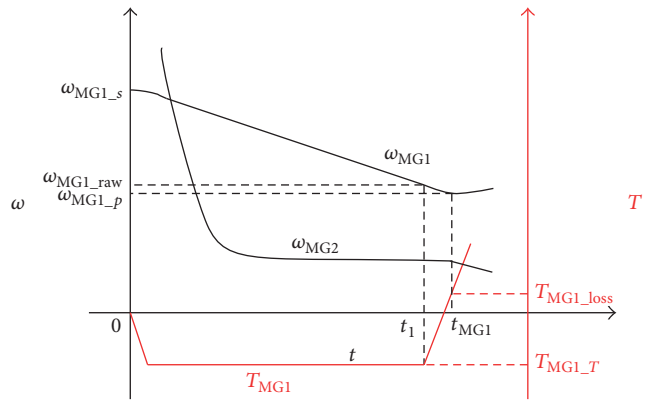

Figure 6: Variables changing curves in upshift speed regulation 2.

MG1 speed does not need to be regulated during downshift process. MG1 only needs to make preparations to unload and put into target gear. In summary, the flow chart of shift speed regulation process is as shown in Figure 7.

3.3. Synchronization Phase. Mechanical speed synchronization is executed by the synchronizer to put into the target gear from neutral gear in this phase, during which shift motor drives the synchronizer to reach the stroke range of the target gear. Hybrid control unit (HCU) adjusts the pulse duty ratio of 24 V voltage to control the power of shift motor in order to overcome the different situations. Moreover, PID control of position and velocity closed loop is utilized to solve the nonlinear and parameter uncertainty situation in mechanical synchronization. If the synchronization time exceeds normal default value, it means that motor stalling appears due to speed regulation failure or shift motor faults. Shift motor has to be stopped immediately at this moment. The shift process interrupts and enters fault mode, where the target gear is revised to neutral gear due to the fact that the resistance to neural gear is relatively small and no contact exists between synchronizer and powertrain in neural gear so as to protect the shift mechanism and check fault reason in park condition. After returning to neutral gear, the shift synchronizer can try to put into the target gear again up to three times. If three attempts all end in failure, then fault lamp is lightened and the gear fixes in neural gear. The flow chart of synchronization phase is shown in Figure 8.

4. Experiments Validation

In order to prepare for the on-board road test, a hybrid electric system bench test-bed was built to debug and validate the basic characteristics of motors and vehicle function implementation, as shown in Figure 9. It consists of coupling system (including two motors and transmission), DMCMs, dynamometer, battery, engine, and accessories.

4.1. Motor Dynamic Characteristic Test on Bench Test-Beds. It can be concluded from (23) and (30) that parameters J, k, and T_{loss} must be confirmed to attain the optimal command

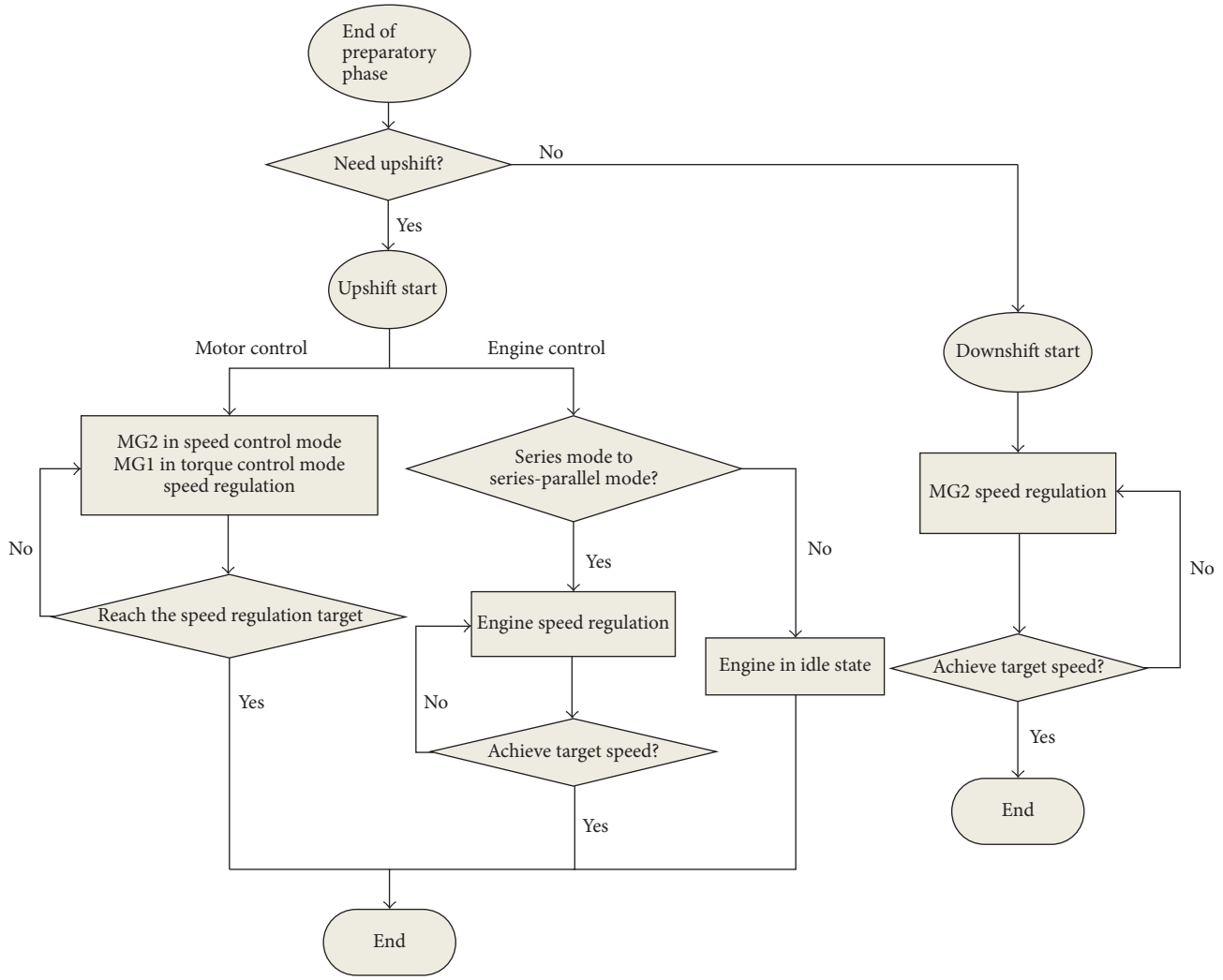

Figure 7: The speed regulation phase's flow chart.

torque T^*. As a series of MG1 free-fall curves under different initial speed conditions shown in Figure 10, in the initial period of time, all the MG1 speed curves are approximated to a straight line of the same slope in the shift speed range. The kinetic equation is shown as follows:

$$T_{\text{loss}} = J\frac{\Delta\omega}{\Delta t}. \tag{32}$$

T_{loss} can be obtained by MG1 torque in its stable speed control mode state. As verified by experiment, in MG1 speed range during shift process, T_{loss} is about 15 Nm. The slope of MG1 free-fall curves is around 19.4 rad/s^2 from Figure 10.

J is 0.77 kg $*$ m^2 from (32). It is far more than the normal rotational inertia of rotors in permanent magnet motors. That is because MG1 transmission shaft is always linked to the ring gear in planetary gear system. Besides, planet gear and carrier are also rotating when MG1 rotates alone. Hence J is actually the sum of MG1 rotational inertia and planetary gear system equivalent rotational inertia. k is 2500 as motor torque response rate is 100 Nm/40 ms according to the motor control requirement. By calculating on the basis of the optimization algorithm mentioned above, ω^*_{MG1} is 1200 rpm. ω^s_{MG1} is 1300 rpm during series mode to series-parallel mode.

T^* is 509 Nm obtained from (23) in the first upshift speed regulation. To verify the validity of the torque value T^*, the relationships of total regulation time t_{MG1} and speed difference $\Delta\omega_{\text{MG1}}$ with unload speed $\omega^{\text{raw}}_{\text{MG1}}$ under different command torque conditions are recorded by experiments. The results are displayed in Figures 11 and 12.

It can be concluded that t_{MG1} and $\Delta\omega_{\text{MG1}}$ are inter-restricted with each other from Figures 11 and 12. Short t_{MG1} requires T^T_{MG1} to be large enough, which will result in large $\Delta\omega_{\text{MG1}}$. On the contrary, small T^T_{MG1} signifies small $\Delta\omega_{\text{MG1}}$, but speed regulation process will be prolonged and the whole shift process will be postponed accordingly. By comparing the results of several sets of data, T^* around 500 Nm can be regarded as the selected command torque comprehensively considering its fast speed regulation and acceptable increase of speed, which is also consistent with the calculation results

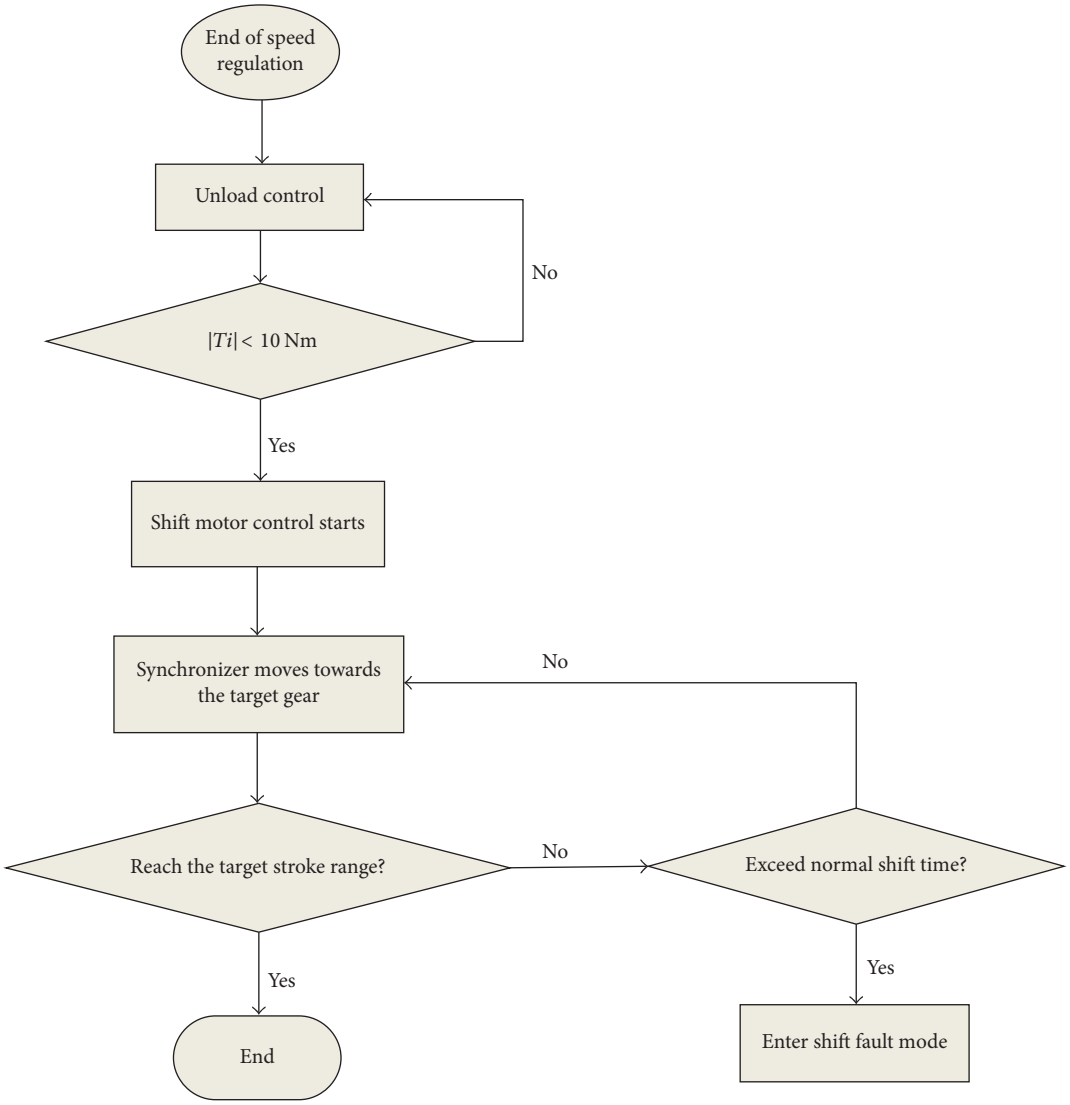

Figure 8: The synchronization phase's flow chart.

Figure 9: Bench test-bed for new hybrid electric system.

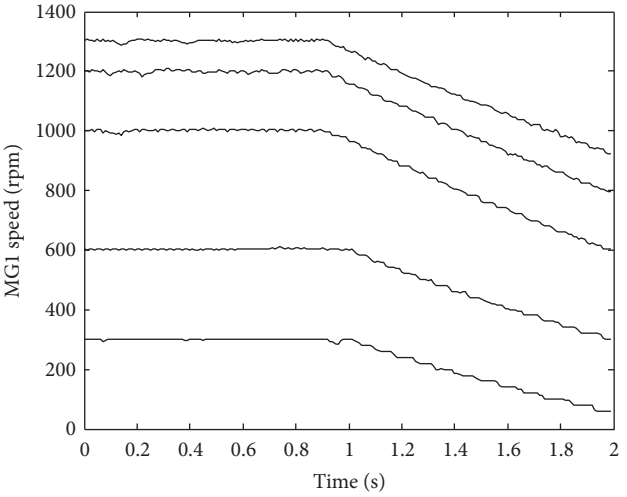

Figure 10: MG1 free-fall speed curves.

from (23). As T^* goes on increasing, the time contraction effect is not obvious, whereas $\Delta\omega_{MG1}$ increases significantly.

In the second upshift speed regulation, T^* is 158 Nm as calculated from (30). Reducing $\Delta\omega_{MG1}$ is considered as the

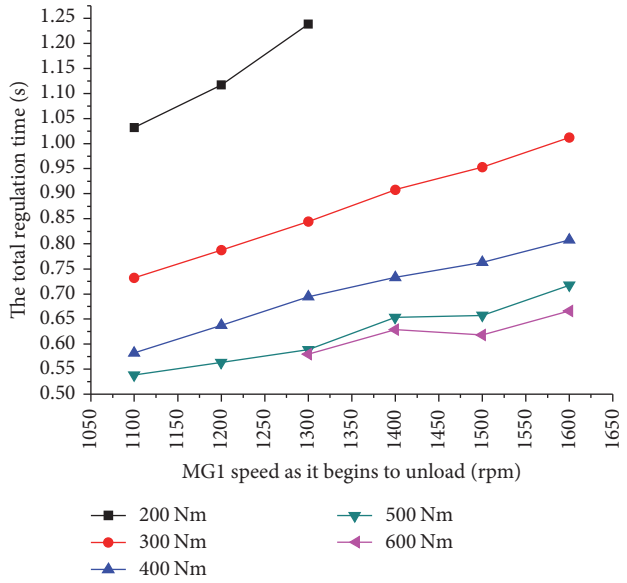

FIGURE 11: The curves of ω_{MG1}^{raw} and t_{MG1} under different T_{MG1}^{T}.

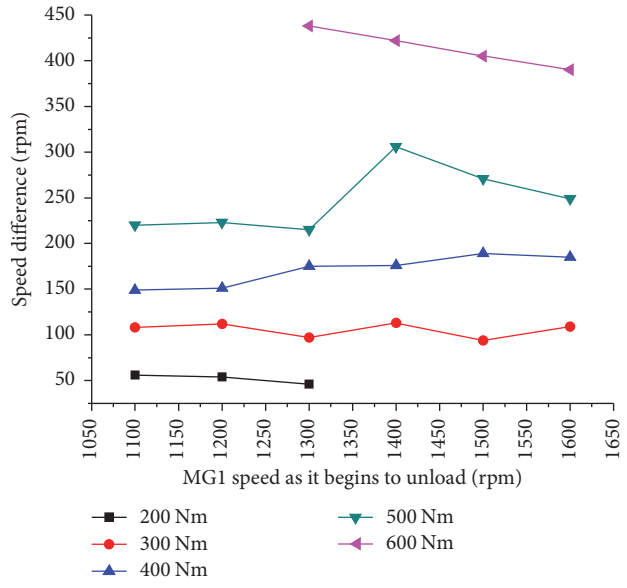

FIGURE 12: The curves of ω_{MG1}^{raw} and $\Delta\omega_{MG1}$ under different T_{MG1}^{T}.

main target at the moment due to the fact that the speed regulation time is relatively small.

ω_{MG1}^{raw} can be obtained from (33) after T_{MG1_T} and ω_{MG1}^{p} are confirmed:

$$\omega_{MG1}^{raw} = \omega_{MG1}^{p} - \frac{\left(T_{loss} - T_{MG1}^{T}\right)^2}{2J_{MG1}k}. \quad (33)$$

In practical engineering application, ω_{MG1}^{raw} can be determined by calibration tests directly. Given $T_{MG1}^{T} = T^*$ as the condition, ω_{MG1}^{p} can be recorded by unloading from a set of

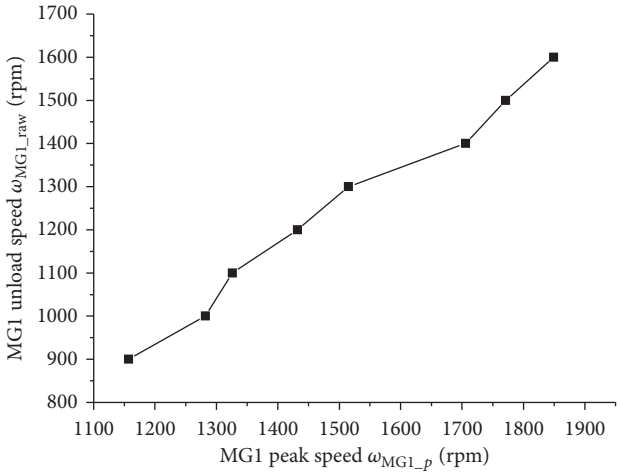

FIGURE 13: The peak speed ω_{MG1}^{p} with unload speed ω_{MG1}^{raw}.

different ω_{MG1}^{raw}. A one-dimensional map was made on basis of the data. ω_{MG1}^{raw} can be gained by the known ω_{MG1}^{p} looking up the map backwards. Taking the first upshift mode as an example, $T^* = 509$ Nm; the map is shown in Figure 13.

Meanwhile, speed control test for MG2 speed characteristics was carried out to make sure that MG2 speed response is fast and accurate. A series of MG2 speed regulation tests were implemented throughout the speed range of shift process. The test results suggest that most of MG2 speed regulation ends in 0.5 s with high accuracy and regulating requirements are satisfied.

The shift success rate was highest when δ and ξ were determined to be 10 rpm and 40 rpm by carrying on the tests about output shaft speed difference in (9). The vibration and noise are also in acceptable level.

4.2. Simulation Test. To prove the effectiveness of the proposed method, a simulation test was operated based on AMESim (Advanced Modeling Environment for performing Simulations of engineering systems). Since the maximum impact degree during the shift process mainly relies on the speed regulation phase and synchronization phase, the upshift procedure from single-motor mode to dual-motor mode was chosen as the simulation object. The simulation architecture diagram of the proposed method was built based on the powertrain transmission solution demo of AMESim, as shown in Figure 14.

The normal force applied on the sleeve of the synchronizer was obtained by the PID method to track an optimal sleeve displacement curve. Meanwhile a normal method without speed regulation phase was simulated to compare the effects, whose structure is shown in Figure 15.

The simulation results of both methods are listed in Figures 16–18. The 0.3 s ahead in proposed method was occupied by speed regulation and the synchronization times in both methods are 0.3 s. Due to the fact that the synchronization time is constant (based on the displacement curve), the impact degree can reflect the drivability performance. It denotes the variation rate of vehicle longitudinal acceleration

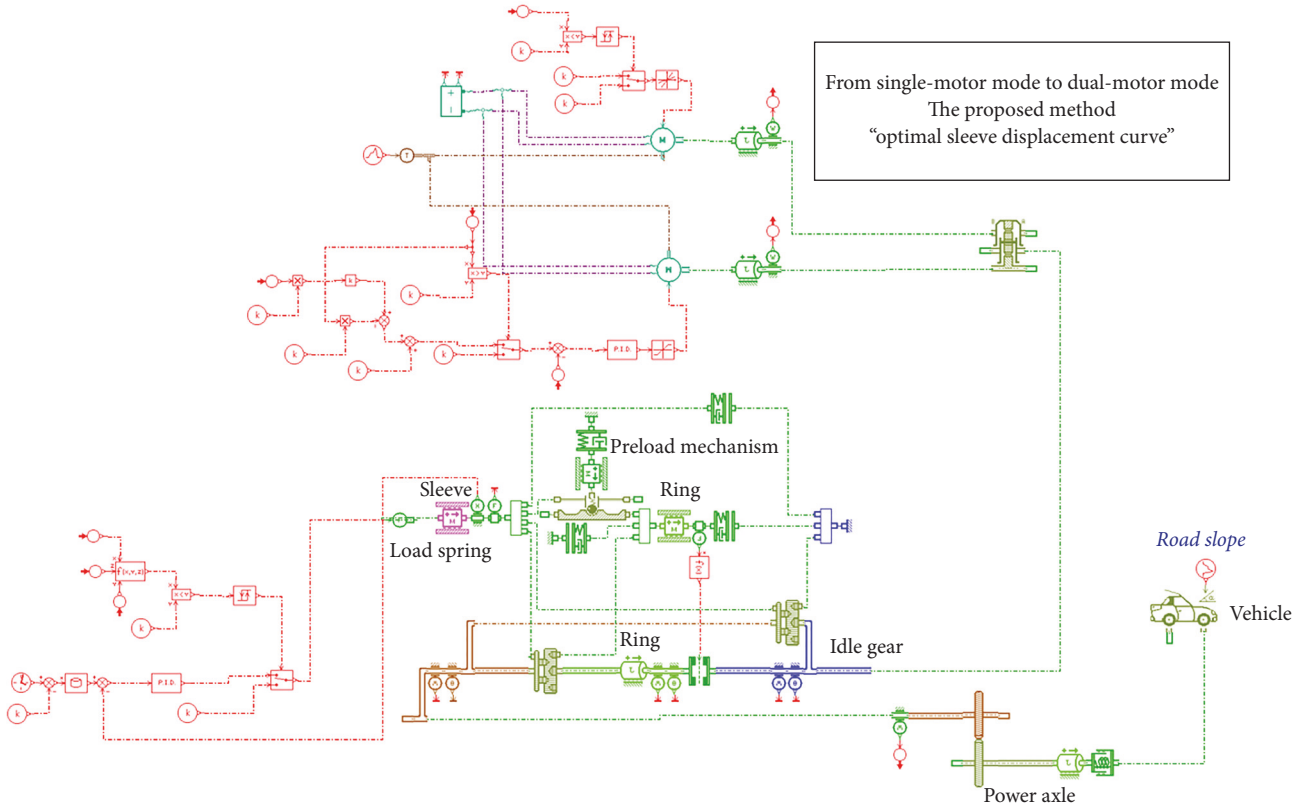

Figure 14: The simulation architecture diagram of the proposed method.

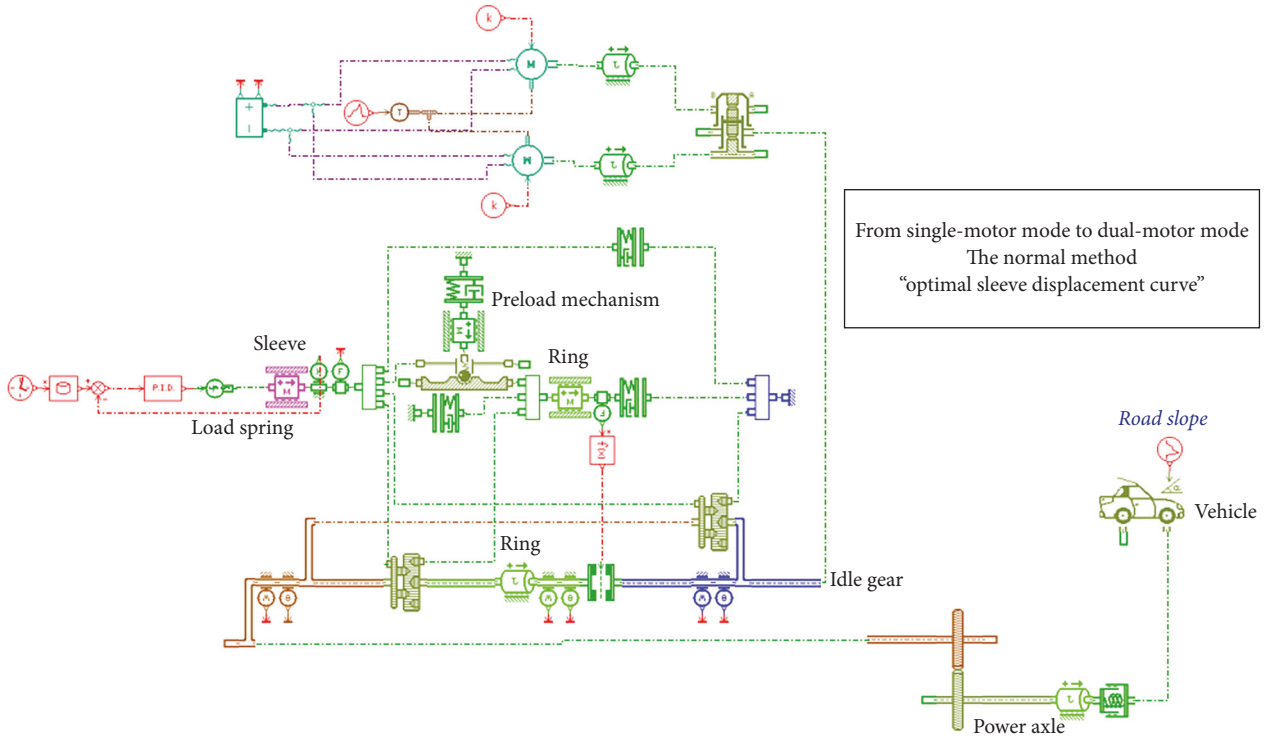

Figure 15: The simulation architecture diagram of the normal method without speed regulation.

Table 2: Definitions of clutch and gear states.

Clutch states	Definitions	Gear states	Definitions
1	Clutch is disengaged	1	At gear 1
2	Clutch is slipping	2	At gear 2
3	Clutch is engaged	0	At gear 0
		3	In shift process

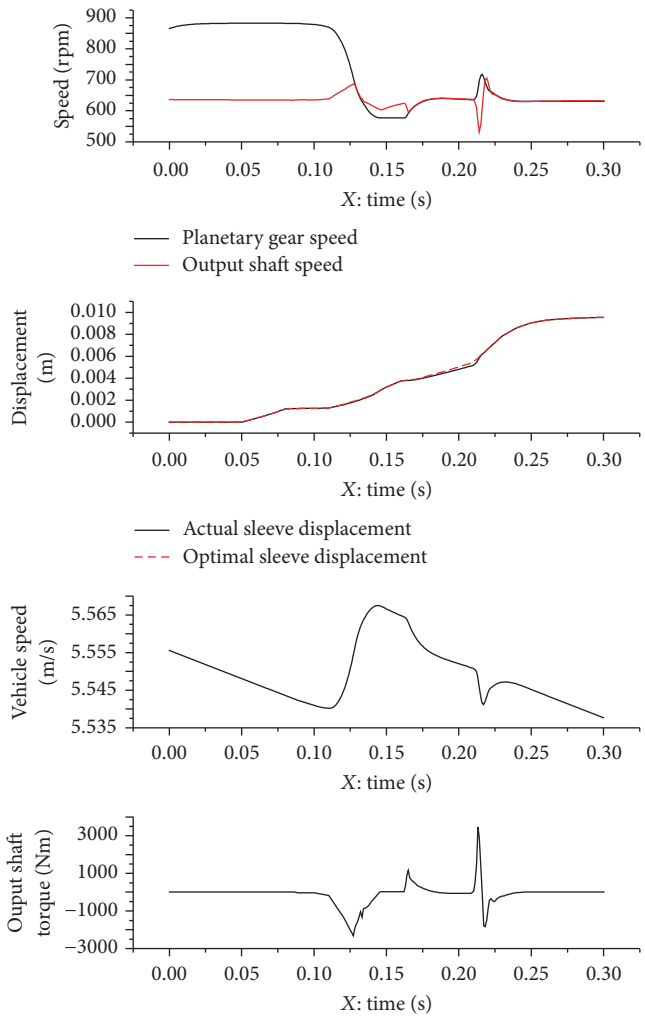

Figure 16: The simulation results of the normal method without speed regulation.

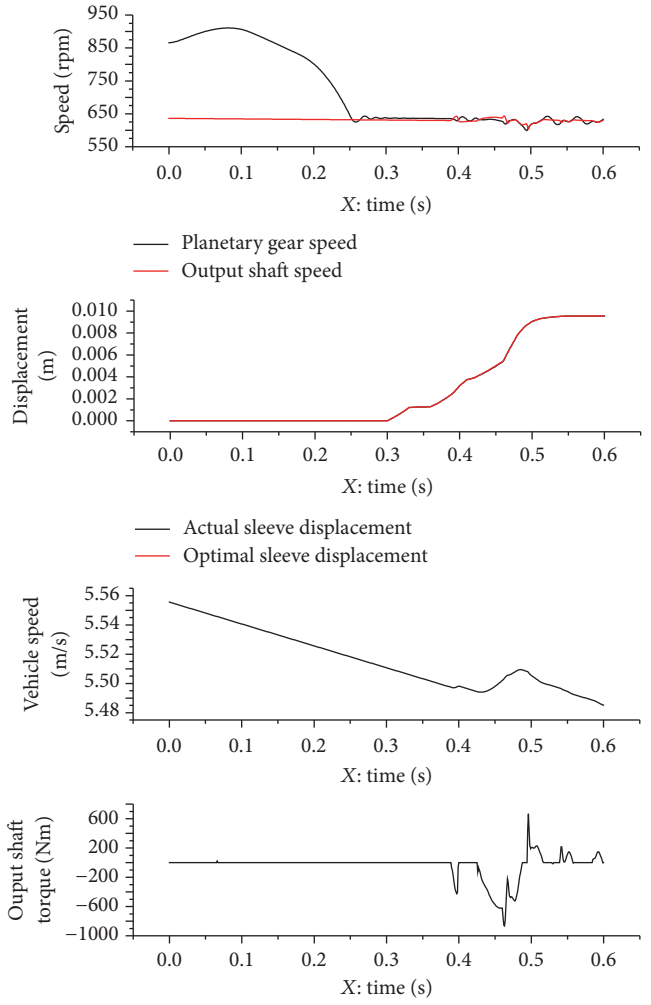

Figure 17: The simulation architecture diagram of the proposed method.

and embodies driver's feeling about the impact load directly and quantitatively, as shown in the following equation:

$$J = \frac{da}{dt} = \frac{d^2v}{dt^2}. \tag{34}$$

On the other hand, another simulation based on a constant force exerted on the sleeve of the synchronizer was operated. The results are shown in Figure 19. The synchronization times of the proposed method and normal method are 0.354 s and 0.544 s, respectively. And the maximum impact degrees are 4.08 m/s^3 and 20.7 m/s^3, respectively.

The two simulation results can verify that the speed regulation phase influences the drivability performance significantly and the proposed method can restrain the impact degree and accelerate the synchronization process remarkably.

4.3. Road Test. The vehicle carrying the new hybrid electric system is shown in Figure 20.

4.3.1. Upshift Test. Clutch states and gear states definitions are listed in Table 2.

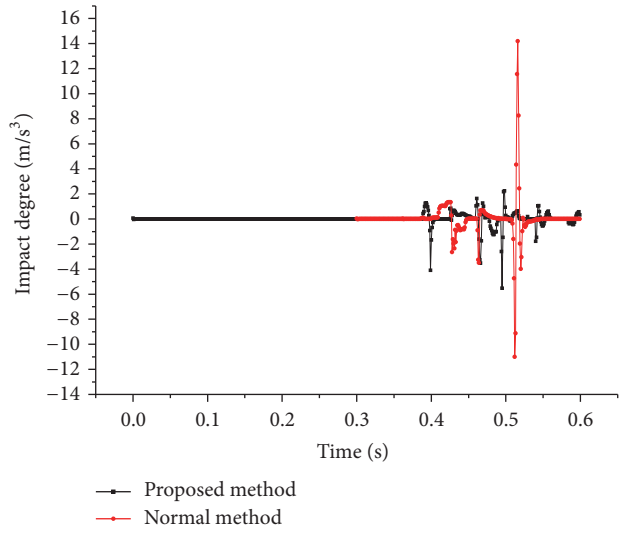

Figure 18: The impact degree curves of the proposed method and normal method with an optimal displacement curve.

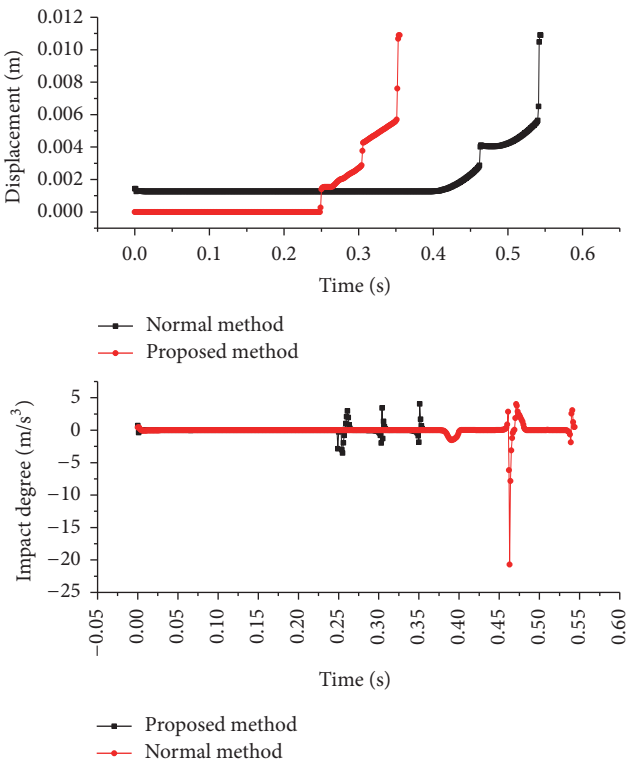

Figure 19: The results of the proposed method and normal method with a constant force.

Considering the space limit, single-motor mode to dual-motor mode is chosen as the research object of upshift process. Clutch state and gear state are displayed in Figure 21. The control commands are in strict accordance with the shifting process execution. The variation curves of speed and torque of two motors are shown in Figure 22. Engine is ignored, since it is in condition of rest.

Figure 20: The vehicle carrying the new hybrid electric system.

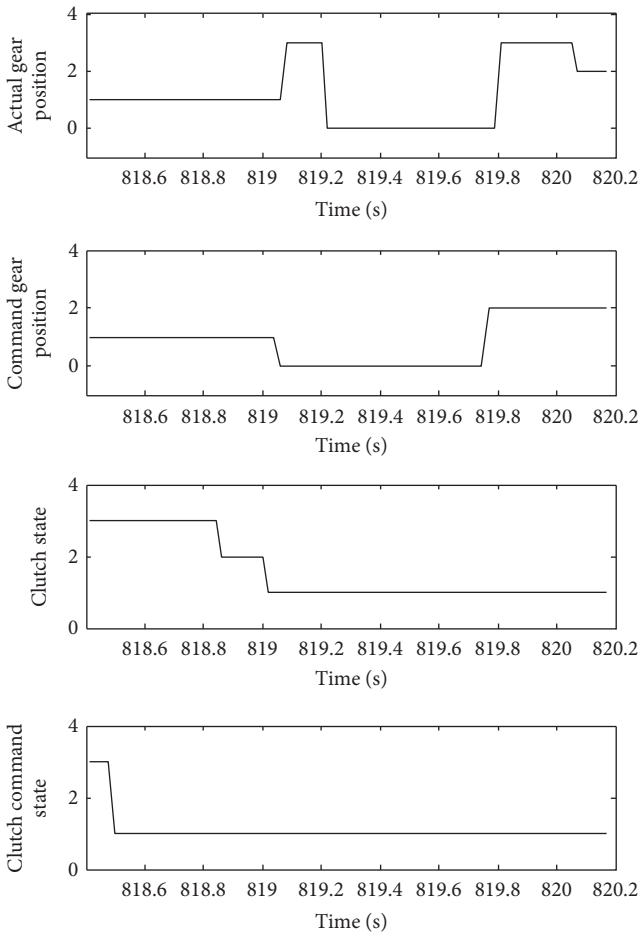

Figure 21: Clutch state and gear state in upshift process.

It can be obtained that, after clutch disengages actually, the command gear turns to neutral gear and the shift mechanism begins to move towards the neutral gear. Then motor speed regulation begins in the neutral gear. MG1 command torque is 500 Nm, which is cleared to zero after MG1 actual speed reaches 969 rpm. The actual torque of MG1 decreases to zero when MG1 speed attains 1182 rpm. MG2 speed is 2952 rpm as the gear position just turns to the neutral gear. MG2 command speed is 0 rpm at the beginning.

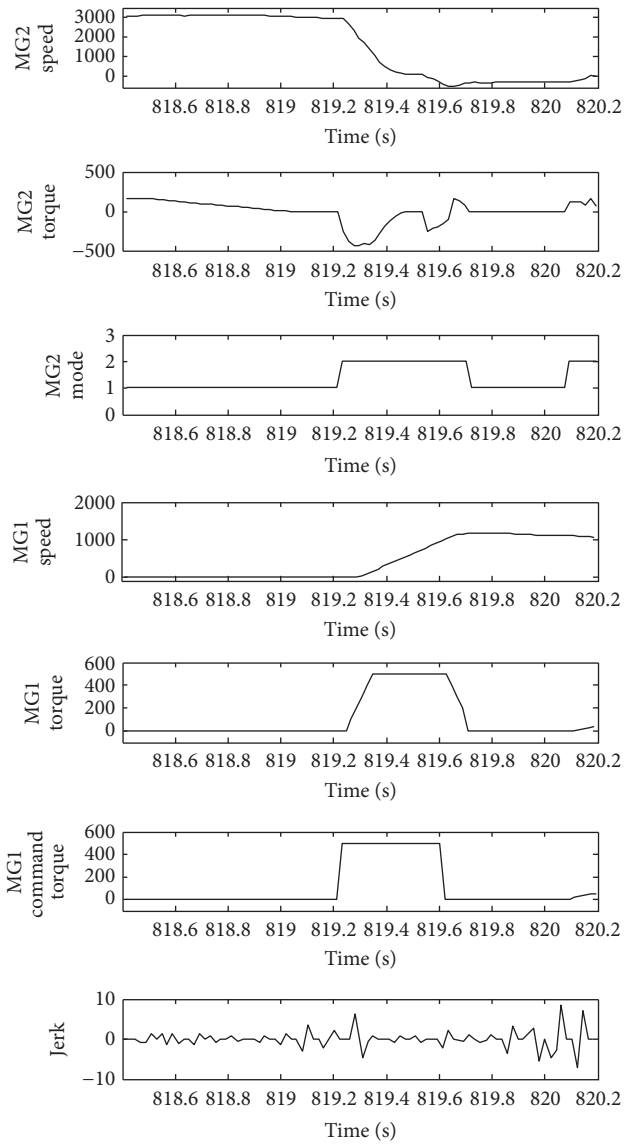

Figure 22: The variation curves of speed and torque of two motors.

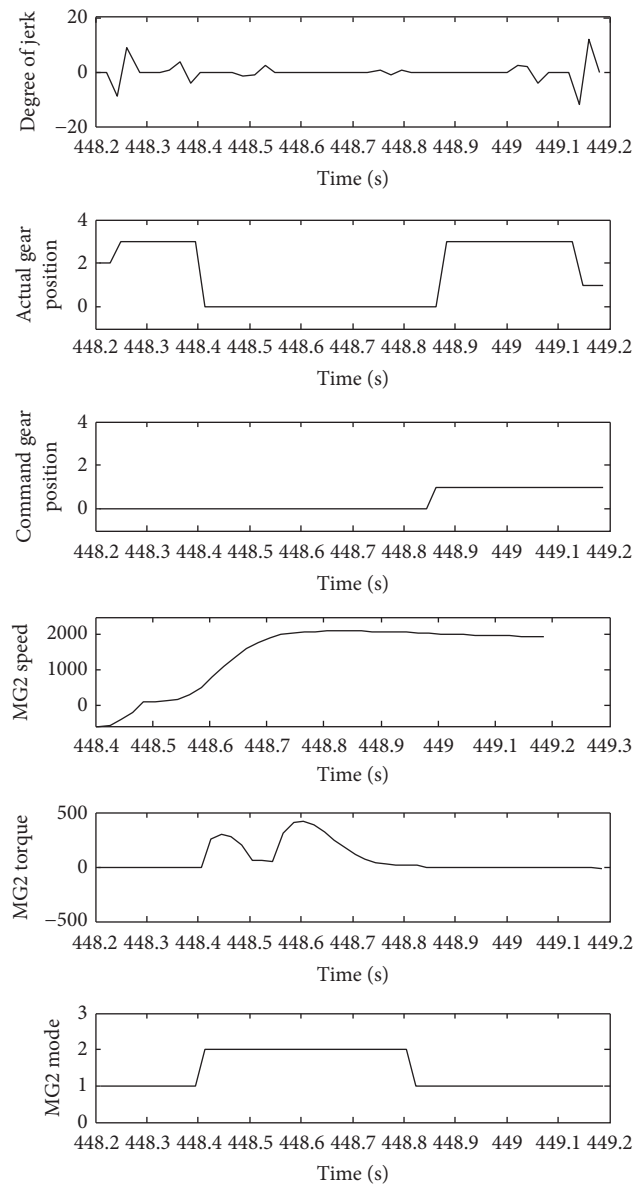

Figure 23: The parameters curves during downshift process.

Then MG2 command speed direction changes from 0 to 1 when its speed is below 200 rpm. MG2 speed reverses as the speed direction is 1. The value of MG2 command speed is calculated by (24). It is first based on MG1 peak speed and its command speed changes as MG1 speed starts to free fall. After MG1 and MG2 speed regulation finishes, the relationship in (9) is satisfied. Then motor torque is cleared and mechanical synchronization begins. The shift mechanism starts to migrate into the target gear.

The total shift process costs 1.08 s in the road test results. MG1 speed is 1170 rpm and MG2 speed is −321 rpm after speed regulation process finishes. The coupling speed ω_s^T is 714 rpm and output shaft speed ω_s is 690 rpm at this time. The speed difference is 24 rpm, which meets the requirement of (9).

The degree of jerk during the shift process is recorded as well. The test results in Figure 22 indicate that the maximum degree of jerk is 8.42 m/s^3, which is smaller than Chinese standard ($J < 17.64$ m/s^3). So the comfort requirements are met during the upshift process.

4.3.2. Downshift Test. The downshift process mainly refers to MG2 speed regulation. MG1 and engine are at idle state. MG2 speed regulation process is shown in Figure 23.

MG2 speed direction is changed from reverse to forward in the neutral gear. The target speed is regulated according to (31). MG2 control mode is tuned from speed control to torque control after speed regulation. Then MG2 starts to unload by clearing MG2 torque to zero. When the actual torque reaches zero, mechanical synchronization starts.

The total downshift time is 0.919 s. At the end of speed regulation, MG2 speed ω_{MG2}^T is 2107 rpm. ω_s^T is 469 rpm by

Table 3: Upshift and downshift on-board experiments results.

Methods	Powertrain	Shift time (s)	Max jerk (m/s^3)
Dynamic coordinated control	Conventional AMT & planetary gear train	Upshift 1.08 Downshift 0.92	Upshift 8.42 m/s^3 Downshift 11.96 m/s^3
Motor speed feedback control	AMT with dual clutch	Upshift 1.24 Downshift 0.72–0.83	Upshift 13.2 rad/s^3 Downshift 82.5 rad/s^3
Without disengaging clutch	Conventional AMT	1.35–1.41	9–12.3 m/s^3
Combined algorithm	Conventional AMT	Upshift 1.20 Downshift 1.10	—

calculation in (2). Output shaft actual speed ω_s is 457 rpm, which is 12 rpm less than ω_s^T. As a result, the speed regulation is effective and (9) can be met. Besides, the degree of jerk during downshift process also meets the smooth standard.

Many methods are presented in other literatures about gear-shift process with different structures, such as the combined gear-shifting method assisted by motor speed feedback control [5], control strategy without disengaging clutch [16], and combined control algorithm based on feed-forward, bang-bang, and PID control [7]. The results are listed in Table 3. Compared with other approaches and structures, the new hybrid system's structural change during gear-shift is more complex, but the jerk and power interruption time are less than others, which can validate that the proposed dynamic shift coordinated control can inhibit vehicle jerks and vibrations during short shift time intervals.

5. Conclusion

A new type of hybrid electric system is utilized to conduct the experiments of shift control and verify the validity of the proposed dynamic shift coordinated control. Motor active speed regulation is required to keep the speed difference between two ends of synchronizer under acceptable level to meet the demand of vibrations and shift success rate. The simulation and road test results proved that, compared with other approaches, the degrees of jerks in both upshift and downshift processes were restrained more effectively, with the shift time interval being shorter as well. Besides, the robustness in conventional AMT and planetary gear train can be validated by tests results during downshift and upshift processes. So far, the situation where vehicle speed dramatically changes during shift process has not been taken into consideration, especially shift in ramp ways. This is also the research direction and focus in the future.

Conflicts of Interest

The authors declare that there are no conflicts of interest regarding the publication of this paper.

References

[1] D. Xiao-feng, H. Yan-qing, Y. Ting, and Y. Lin, "Research on Power Split Strategy Based on Fuzzy Logic Control Strategy for a Four-mode Hybrid Electric Bus [J]," *Mechatronics*, vol. 03, pp. 13–19, 2015.

[2] M. Pei-pei, Y. Bin, H. Yan-qing, and Y. Lin, "Energy Management Optimization for New Hybrid Electric System [J]," in *Vehicle Engine*, vol. 6, pp. 1–6, 2013.

[3] C. Liang, Z. Hao, L. YANG, and H. Yan-qing, "Vehicle control and simulation study of new HEV [J]," *Chinese Journal of Power Sources*, vol. 4, pp. 846–848, 875, 2016.

[4] H.-D. Lee, S.-K. Sul, H.-S. Cho, and J.-M. Lee, "Advanced gear-shifting and clutching strategy for a parallel-hybrid vehicle," *IEEE Industry Applications Magazine*, vol. 6, no. 6, pp. 26–32, 2000.

[5] L. Glielmo, L. Iannelli, V. Vacca, and F. Vasca, "Gearshift control for automated manual transmissions," *IEEE/ASME Transactions on Mechatronics*, vol. 11, no. 1, pp. 17–26, 2006.

[6] S. Shin, J. Oh, J. Kim, and S. Hong, "A method of gear-shift in parallel hybrid electric vehicle using motor control," *SAE Technical Papers*, 2010.

[7] R. C. Baraszu and S. R. Cikanek, "Torque fill-in for an automated shift manual transmission in a parallel hybrid electric vehicle [C]," in *Proceedings of the American Control Conference*, vol. 2, pp. 1431–1436, May 2002.

[8] V. Ngo, T. Hofman, M. Steinbuch, and A. Serrarens, "Predictive gear shift control for a parallel hybrid electric vehicle," in *Proceedings of the 7th IEEE Vehicle Power and Propulsion Conference (VPPC '11)*, pp. 1–6, IEEE, Chicago,Ill, USA, September 2011.

[9] Y.-S. Yoon, S. J. Kim, and K.-S. Kim, "Conceptual design of economic hybrid vehicle system using clutchless geared smart transmission," *International Journal of Automotive Technology*, vol. 14, no. 5, pp. 779–784, 2013.

[10] C.-H. Yu, C.-Y. Tseng, and C.-P. Wang, "Smooth gear-change control for EV Clutchless Automatic Manual Transmission," in *Proceedings of the 2012 IEEE/ASME International Conference on Advanced Intelligent Mechatronics, AIM 2012*, pp. 971–976, twn, July 2012.

[11] C.-H. Yu and C.-Y. Tseng, "Research on gear-change control technology for the clutchless automatic-manual transmission of an electric vehicle," *Proceedings of the Institution of Mechanical Engineers, Part D: Journal of Automobile Engineering*, vol. 227, no. 10, pp. 1446–1458, 2013.

[12] J. Li, H. Wei, F. Sun, and C. Zhang, "Coordinated control of downshift powertrain of combined clutch transmissions for electric vehicles," in *Proceedings of the 6th International Conference on Applied Energy, ICAE 2014*, pp. 1917–1920, twn, June 2014.

[13] Z. Zhong, G. Kong, Z. Yu, X. Xin, and X. Chen, "Shifting control of an automated mechanical transmission without using the

clutch," *International Journal of Automotive Technology*, vol. 13, no. 3, pp. 487–496, 2012.

[14] H. Liu, Y. Lei, Z. Li, J. Zhang, and Y. Li, "Gear-Shift Strategy for a Clutchless Automated Manual Transmission in Battery Electric Vehicles," *SAE International Journal of Commercial Vehicles*, vol. 5, no. 1, pp. 57–62, 2012.

[15] Y. Yun-yun, W. Seng, and F. Xiang, "Shifting control algorithm for a single-axle parallel plug-in hybrid electric bus equipped with EMT [J]," *Discrete Dynamics in Nature and Society*, 2014.

[16] H. Yu, J. Xi, F. Zhang, and Y. Hu, "Research on gear shifting process without disengaging clutch for a parallel hybrid electric vehicle equipped with AMT," *Mathematical Problems in Engineering*, vol. 2014, Article ID 985652, 12 pages, 2014.